Numerical Simulation of the Shoreline Modifications behind a T-Head Groin

Francesco Gallerano
Department of Civil, Constructional and Environmental Engineering "Sapienza" University of Rome
Via Eudossiana 18, 00184
ITALY
+39 0644585062
francesco.gallerano@uniroma1.it

Marco Tamburrino
Department of Civil, Constructional and Environmental Engineering "Sapienza" University of Rome
Via Eudossiana 18, 00184
ITALY
+39 0644585062
marco.tamburrino@uniroma1.it

ABSTRACT
In this paper, the shoreline and bottom modifications produced by the presence of a T-head groin are simulated. We present a model for the bottom-change simulation, composed by two sub-models: a two-dimensional phase-resolving model for the simulation of the variation of the fluid dynamic variables inside the wave period and that takes into account the undertow; a second morphodynamic sub-model for the simulation of the bottom changes, in which the suspended sediment concentration is calculated by means of the wave-averaged advection-diffusion equation. Both the fluid motion equation and the concentration equation are written in a new contravariant formulation. We simulate the velocity fields from deep water to the start of the surf-zone by a new integral contravariant form of the Fully Nonlinear Boussinesq Equations. We simulate the bed evolution dynamics by means of the contravariant formulation of the advection–diffusion equation for the suspended sediment concentration. A quasi three-dimensional approach is used to formulate the advective sediment transport terms in the advection-diffusion equation.

CCS Concepts
• Applied Computing Physical Sciences and Engineering→Engineering.

Keywords
Phase-resolving model; undertow; intra-wave quantities; concentration equation; sediment transport; sea bottom modification.

1. INTRODUCTION
The sea bottom modifications induced by coastal structures can be predicted by simulating velocity fields and suspended sediment concentration fields. Unfortunately, three-dimensional simulations [1-3] require a lot of computational time and cannot be used for long-time sea bottom simulations.

The two-dimensional phase-resolving models, not averaged over the wave period are based on the solution of the Boussinesq equations, which are obtained by defining the depth dependence of the variables, and by depth integrating the motion equations.

In this context, numerical models based on shock-capturing schemes that numerically integrate both the Fully Nonlinear Boussinesq Equations (hereinafter called FNBE's) [4,9] and nonlinear shallow-water equation (hereinafter called NSWE), allow explicit simulations of wave breaking [10].

Bottom changes in the coastal region are produced by complex hydrodynamic processes. The resuspension of the solid particles and their transport and settling are driven by the hydrodynamic quantities that vary in the wave period.

In this paper, in order to simulate hydrodynamic fields from deep water to the start of the surf zone, a new integral contravariant form of the FNBE's is proposed. The abovementioned motion equations retain the term related to the second-order vertical vorticity. Inside the surf zone, breaking wave propagation is simulated by integrating the NSWE.

Dispersive terms are not present in the integral form of the proposed continuity equation, so that this equation can be entirely discretized by a shock-capturing finite volume scheme: doing so, the errors due to the low-order discretization of such dispersive term are not present into the solution.

Bed evolution dynamics is calculated from the contravariant formulation of the advection–diffusion equation for the suspended sediment concentration. The advective sediment transport terms that appear in the above equation are formulated according to a quasi-three-dimensional approach [11,12] (hereinafter called Q3D) and are calculated starting from the depth-integrated product of the horizontal velocity and concentration the vertical distributions, in order to take into account, the sediment transport related to the undertow. The bottom variation over time is related to the contribution given by the product of the settling velocity and the difference between reference concentration and actual concentration (at a given distance a from the bottom) and to the contribution given by the spatial variation of the bed load transport.

2. GOVERNING EQUATIONS

2.1 Hydrodynamic Model
Let $H = h + \eta$ be the total local water depth, where h is the local still water depth and η is free surface elevation with respect to the undisturbed free surface. Let σ be an arbitrary distance from the still water surface. By using a Taylor expansion of the velocity

Permission to make digital or hard copies of part or all of this work for personal or classroom use is granted without fee provided that copies are not made or distributed for profit or commercial advantage and that copies bear this notice and the full citation on the first page. Copyrights for third-party components of this work must be honored. For all other uses, contact the Owner/Author.
ICCTA '20, April 14–16, 2020, Antalya, Turkey
© 2020 Copyright is held by the owner/author(s).
ACM ISBN 978-1-4503-7749-2/20/04…$15.00
https://doi.org/10.1145/3397125.3397132

about σ and by assuming zero horizontal vorticity, the vertical distribution of the horizontal velocity $\vec{U}(z)$ can be written as

$$\vec{U}(z) = \vec{u} + \vec{v}(z) \tag{1}$$

In equation (1), $\vec{u}$ is the horizontal velocity at $z = \sigma$ and $\vec{v}(z)$ represents the second order term in power series expansion of the velocity vector about σ, in which ∇ is the two-dimensional differential operator defined as $\nabla = \left(\frac{\partial}{\partial x}, \frac{\partial}{\partial y}\right)$ in a Cartesian reference system,

$$\vec{v}(z) = (\sigma - z)\nabla\left(\nabla \cdot (h\vec{u})\right) + \left(\frac{\sigma^2}{2} - \frac{z^2}{2}\right)\nabla(\nabla \cdot (\vec{u})) \tag{2}$$

We define $\vec{\bar{v}}$ as the depth averaged value of $\vec{v}(z)$, obtained by retaining terms of order $O(\mu^2, \varepsilon^2\mu^2)$, which is

$$\vec{\bar{v}} = \frac{1}{H}\int_{-h}^{\eta} \vec{v}(z)\, dz = \left(\frac{\sigma^2}{2} - \frac{1}{6}(h^2 - h\eta + \eta^2)\right)\nabla\left(\nabla \cdot (\vec{u})\right) + \left(\sigma + \frac{1}{2}(h - \eta)\right)\nabla(\nabla \cdot (h\vec{u})) \tag{3}$$

Let $x^l = x^l(\xi^1, \xi^2)$ (with *l=1,2)* be the transformation from the Cartesian coordinate system $\vec{x}$ to the curvilinear coordinate system $\vec{\xi}$ (henceforth the superscript indicates components and not powers). Let $\vec{g}_{(l)} = \partial\,\vec{x}/\partial\,\xi^l$ be the covariant base vector and $\vec{g}^{(l)} = \partial\,\xi^l/\partial\,\vec{x}$ be the contravariant base vector. The metric tensor and its inverse are given respectively by $g_{lm} = \vec{g}_{(l)} \cdot \vec{g}_{(m)}$ and $g^{lm} = \vec{g}^{(l)} \cdot \vec{g}^{(m)}$. The Jacobian of the transformation is $\sqrt{g} = \sqrt{det(g_{lm})}$. The transformation relationships between the components of the generic vector $\vec{b}$ in the Cartesian coordinate system and its contravariant and covariant components, b^l and b_l, in the curvilinear coordinate system are given in the Appendix. In order to apply a shock capturing scheme to the Boussinesq type equations, the convective terms must be expressed in conservative form, i.e. in divergence form. In [4] the system evolution variables were the conserved variables H and Hu^l. Using these conserved variables implies the presence of a source term in the mass conservation equation (right-hand side of equation (4) in [4]). In order to avoid it, in this paper the conserved variables are the total local depth H and the following contravariant quantity

$$M^l = H(u^l + \bar{v}^l) \tag{4}$$

in which $(u^l + \bar{v}^l)$ represents the depth averaged horizontal velocity; u^l and $\bar{v}^l$ are the contravariant components of the vectors $\vec{u}$ and $\vec{\bar{v}}$. With these choices, following the procedure described in [13], we can derive the integral form of the continuity equation and of the momentum equation.

Over the element of area ΔA, the integral form of the continuity equation reads:

$$\frac{\partial \tilde{H}}{\partial t} = -\frac{1}{\Delta A}\sum_{\mu=1}^{2}\left[\int_{\Delta\xi^{\mu+}} M^{\mu}\sqrt{g}\,d\xi^{\nu} - \int_{\Delta\xi^{\mu-}} M^{\mu}\sqrt{g}\,d\xi^{\nu}\right] \tag{5}$$

where $\tilde{H}$ represents the average value of H over the surface element of area ΔA.

$$\tilde{H} = \frac{1}{\Delta A}\iint_{\Delta A} H\sqrt{g}\,d\xi^1 d\xi^2 \tag{6}$$

The choice of the conserved variable M^l expressed by equation (4) makes it possible to write the continuity equation without any source term, but only with a flux term (right-hand side of Equation (6)). Over the same element of area ΔA, the integral form of the momentum equation reads

$$\begin{aligned}
&\frac{\partial \tilde{D}^l}{\partial t} = \\
&\frac{1}{\Delta A}\Bigg\{-\sum_{\mu=1}^{2}\Bigg[\int_{\Delta\xi^{\mu+}}\left(\vec{\tilde{g}}^{(l)} \cdot \vec{g}_{(k)}\frac{M^k M^{\mu}}{H} + \vec{\tilde{g}}^{(l)} \cdot \vec{g}^{(\mu)}\, G\frac{\hat{H^2}}{2}\right)\sqrt{g}\,d\xi^{\nu} - \\
&\int_{\Delta\xi^{\mu-}}\left(\vec{\tilde{g}}^{(l)} \cdot \vec{g}_{(k)}\frac{M^k M^{\mu}}{H} + \vec{\tilde{g}}^{(l)} \cdot \vec{g}^{(\mu)} G\frac{\hat{H^2}}{2}\right)\sqrt{g}\,d\xi^{\nu}\Bigg] + \\
&\iint_{\Delta A} G(\eta - \eta_c)\,\vec{\tilde{g}}^{(l)} \cdot \vec{g}_{(k)} g^{km} h_{,m}\sqrt{g}\,d\xi^1 d\xi^2 + \\
&G\eta_c\sum_{\mu=1}^{2}\Bigg[\int_{\Delta\xi^{\mu+}}\vec{\tilde{g}}^{(l)} \cdot \vec{g}^{(\mu)} h\sqrt{g}\,d\xi^{\nu} - \\
&-\int_{\Delta\xi^{\mu-}}\vec{\tilde{g}}^{(l)} \cdot \vec{g}^{(\mu)} h\sqrt{g}\,d\xi^{\nu}\Bigg] + \\
&\frac{G}{2}\sum_{\mu=1}^{2}\Bigg[\int_{\Delta\xi^{\mu+}}\vec{\tilde{g}}^{(l)} \cdot \vec{g}^{(\mu)} \hat{h^2}\sqrt{g}\,d\xi^{\nu} - \\
&\int_{\Delta\xi^{\mu-}}\vec{\tilde{g}}^{(l)} \cdot \vec{g}^{(\mu)} \hat{h^2}\sqrt{g}\,d\xi^{\nu}\Bigg] - \\
&\iint_{\Delta A} H\vec{\tilde{g}}^{(l)} \cdot \vec{g}_{(k)} V''^k\sqrt{g}\,d\xi^1 d\xi^2 - \\
&\iint_{\Delta A} H\vec{\tilde{g}}^{(l)} \cdot \vec{g}_{(k)}(T^k + W^k + R^k)\sqrt{g}\,d\xi^1 d\xi^2 + \\
&\iint_{\Delta A}\vec{\tilde{g}}^{(l)} \cdot \vec{g}_{(k)}\frac{\partial H}{\partial t}(V'^k - \bar{v}^k)\sqrt{g}\,d\xi^1 d\xi^2 + \\
&\iint_{\Delta A} H\left(\vec{\tilde{g}}^{(l)} \cdot \vec{g}_{(k)}\bar{v}^k\right)_{,m} u^m\sqrt{g}\,d\xi^1 d\xi^2 + \\
&\iint_{\Delta A} H\left(\vec{\tilde{g}}^{(l)} \cdot \vec{g}_{(k)}u^k\right)_{,m}\bar{v}^m\sqrt{g}\,d\xi^1 d\xi^2 + \\
&\iint_{\Delta A} H\left(\vec{\tilde{g}}^{(l)} \cdot \vec{g}_{(k)}\bar{v}^k\right)_{,m}\bar{v}^m\sqrt{g}\,d\xi^1 d\xi^2\Bigg\}
\end{aligned} \tag{7}$$

In equation (7), the "^" symbol indicates the operation of power raising and η_c is an arbitrary constant value, G is acceleration due to gravity. R^l, V^l, T^l, W^l are, respectively, the contravariant components bottom resistance term, dispersive terms obtained by retaining terms of order $O(\mu^2, \varepsilon^3\mu^2)$ and term related to the second order approximation of the vertical vorticity. In particular, V^l can be expressed as:

$$V^l = \frac{\partial V'^l}{\partial t} + V''^l \tag{8}$$

See [13] for details on the values of V'^l and V''^l. D^l is an auxiliary variable defined by $D^l = H(u^l + V'^l)$. In equation (7), $\tilde{D}^l$ represent the averaged value of D^l over the surface element of area ΔA, defined as

$$\tilde{D}^l = \frac{1}{\Delta A}\iint_{\Delta A} \mathrm{D}^l\sqrt{g}\,d\xi^1 d\xi^2 \tag{9}$$

Equations (7) and (5) represent a new integral form of the Fully Nonlinear Boussinesq Equations, expressed in a contravariant formulation in which Christoffel symbols are not present. These equations are accurate to $O(\mu^2, \varepsilon^3\mu^2)$ in dispersive terms and conserve vertical vorticity with a leading-order error of $O(\mu^4)$. In the above-mentioned equations the conserved variables are H and M^l. Consequently, the momentum balance equation differs from the one presented by Cannata et al. [4] for the

different expression of the convective terms. Furthermore, unlike the [4] model, no dispersive term is present in the continuity equation. Because of it, the continuity equation can be entirely solved with a high order shock capturing finite volume scheme. In this way, in the numerical solution the errors due to the discretization of the dispersive term in the continuity equation are not introduced. Furthermore, the surface gradient term has been split in order to solve this term by a finite volume technique and to obtain a "well balanced" numerical scheme.

According to [13], the reconstruction of the surface elevation instead of the flow depth can damp spurious oscillations that arise in presence of variable bathymetry. With this procedure, the so-called C-property, i.e. the ability of the scheme to maintain quiescent conditions for a water body at rest, is satisfied. Furthermore, the conserved variable M^l is reconstructed instead of u^l, as suggested by [13]. The numerical reconstructions of M^l can be affected by metric terms. For this reason, in order to eliminate the dependence between the reconstructions and the metric terms, we follow the procedure shown by [13] and we reconstruct vector components with respect to a basis defined by a pair of constant unit vectors.

According to [14], the simulation of the hydrodynamic quantities needed for the solid transport model, requires good shock-capturing and non-oscillatory properties, when there are irregular bed and complex geometries. In this paper, in order to reduce the spurious oscillations in the numerical solution, a different numerical scheme from the one proposed by [14], is adopted. Differently from [14], in this paper, WENO reconstructions are carried out by means of genuinely 2D reconstructions, instead of a dimension by dimension procedure. Indeed, Gallerano et al. [13] showed that genuinely 2D WENO reconstructions offer a better performance in the context of curvilinear complex domains. The reconstruction in the calculation cell $I_{i;j}$ is carried out by means of a convex combination of nine biquadratic polynomials centered in cells adiacent to the calculation cell $I_{i;j}$. Following the WENO procedure, an index of smoothness is computed for each polynomial, in order to evaluate the WENO weights and to obtain the convex combination of the nine polynomials. More details about genuinely 2D reconstructions can be found in [13].

From the integration of the momentum balance equation inside the boundary layer and from the logarithmic law of the velocity profile, follows the procedure of Fredsøe [15], we calculate the intra-wave hydrodynamic quantities, the friction velocity and the thickness of the oscillating turbulent boundary layer.

Under breaking waves, the turbulence is given by the contributions produced by current, wave boundary layer and wave breaking. A turbulent kinetic energy and length scale model is used for the simulation of the turbulent phenomena under breaking wave.

2.2 Morphodynamic Model

The solid particle concentration equation in integral form, in which a quasi-three-dimensional methodology is used, is expressed by

$$\iint_{\Delta A} \frac{\partial \widetilde{C}\widetilde{H}}{\partial t} dA + \int_L \left[\int_a^{\widetilde{H}} \tilde{C}(z)\tilde{u}^r(z)dz \right] n_r dL$$
$$\int_L \bar{\bar{\nu}}_t \widetilde{H} b^{rk} \left(\bar{\tilde{C}}\right)_{,k} n_r dL = \iint_{\Delta A} (P - D) dA \qquad (10)$$

in which $\vec{n}$ is the outward normal vector to the contour line L; $\tilde{C}(z)$ is the solid particle concentration averaged on the wave period; $\widetilde{H}$ is the water depth; $\tilde{u}^r$ is the horizontal contravariant velocity vector averaged over the wave period; a is the distance from the bottom which defines the region in which the bed load transport occurs; $\bar{\bar{\nu}}_t$ is the depth and wave-averaged eddy viscosity; D is the rate of the sediment deposition and P is the rate of turbulent sediment pick-up. D and P are given by

$$D = w_{sed}\tilde{C}_a \qquad (11)$$
$$P = w_{sed}\tilde{C}_R \qquad (12)$$

in which w_{sed} is the sediment fall velocity, $\tilde{C}_a$ and $\tilde{C}_R$ are, respectively, the actual and reference concentrations, that are evaluated at height $a = 2d_{50}$. For the calculation of $\tilde{C}_R$, a threshold value of the sediment particle motion is needed. In order to integrate equation (10), the calculation of $\tilde{C}_a$ and $\tilde{C}_R$ are needed. Let the turbulent suspended sediment diffusion equation be

$$-\tilde{C}(z)w_{sed} = \widetilde{\nu_t}(z)\frac{\partial \tilde{C}(z)}{\partial z} \qquad (13)$$

and the integral that gives the depth-averaged value of $\tilde{C}(z)$ be

$$\bar{\tilde{C}} = \frac{1}{\widetilde{H}} \int_a^{\widetilde{H}} \tilde{C}(z)\, dz \qquad (14)$$

The value of $\tilde{C}_a$ is taken as the lower boundary condition of the following turbulent suspended sediment diffusion Equation (13), and as the lower extreme of the integral in Equation (14). Thus, with the use of Equation (14), where the values of $\bar{\tilde{C}}$ and $\widetilde{\nu_t}(z)$ are known (from the previous time step), an iterative procedure is used to calculate $\tilde{C}_a$,. The value of $\tilde{C}_R$ is obtained by wave-averaging its instantaneous values $C_R(t)$ that are calculated according to [16].

The total transport is given by the sum of the bed load transport, which considers the near bed transport mechanism, and the suspended load transport. The contravariant equation of the bed change expressed in a curvilinear coordinate system is

$$\frac{\partial z_f}{\partial t} = -\frac{1}{1-p}\left[(P - D) + \tilde{q}^k_{b,k}\right] \qquad (15)$$

in which p is the porosity of the sediment and z_f is the elevation of the bed; $\tilde{q}^k_b$ $(k = 1,2)$ is the contravariant components of the bed load transport vector $\tilde{\vec{q}}_b$ proposed by [11].

3. SEA BOTTOM MODIFICATIONS BEHIND A T-HEAD GROIN

In this Section, the Test T3C1 described in the data report by Gravens and Wang [17], is numerically reproduced. Test T3C1 was carried out experimentally on a natural beach with a 4-m long T-head groin centrally located in the alongshore direction of the model beach; the head of the structure is parallel-positioned 4m offshore of the initial shoreline. The Test T3C1 has a duration of 184 min. A random wave is generated by a wave generator, with a 0.26 m significant breaking wave height, a 1.5 s period and an approximate wave angle of 6.5° with respect to the shoreline. In the experiment, the sediment is characterized by a mean diameter of 150 μm. Random wave trains with JONSWAP frequency spectrum and a significant breaking wave height of 0.26 m, are internally generated in the numerical simulation.

Figure 1 illustrates the depth contour lines in the initial condition for Test T3Cl, and the two sections A and B where experimental data are known.

An instantaneous wave field obtained by the numerical simulation of Test T3C1 carried out by the proposed model is shown in Figure 2. It can be noted that, starting from about $x = 15m$ toward the shoreline the breaking causes the wave height to gradually decrease. In the same figure, it can be noted that the wave fronts, in the lee of the T-head groin, undergo a rotation owing to the diffraction effects (although attenuated by the wave breaking).

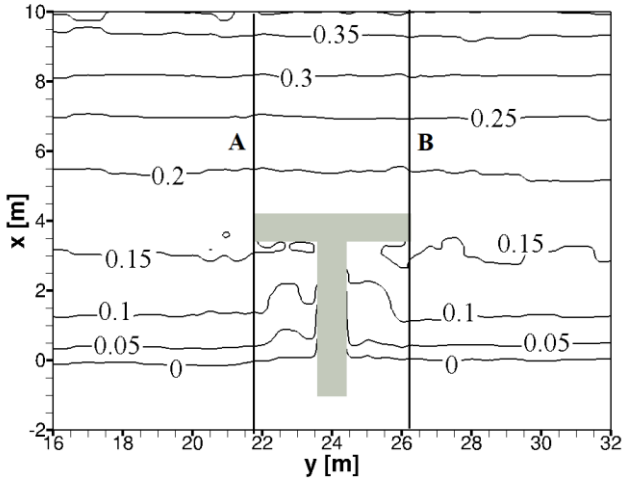

Figure 1 Initial depth contour lines (black solid lines), and comparison sections (black solid line A and B) for Test T3Cl.

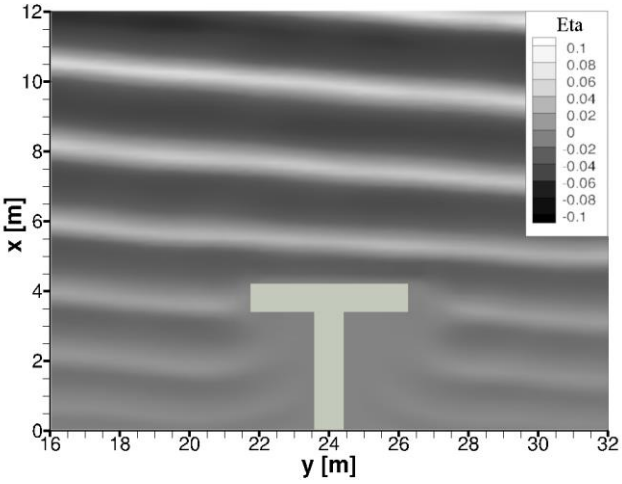

Figure 2 Instantaneous wave field for Test T3Cl.

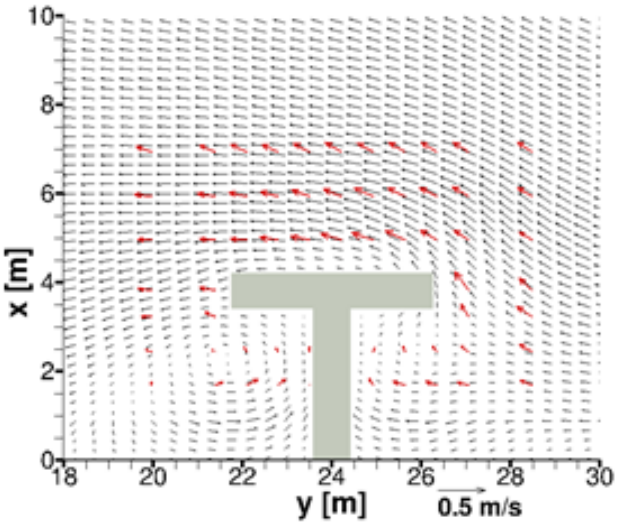

Figure 3 Wave-averaged velocity field: calculated (black vectors) and measured (red vectors) velocity current for Test T3Cl.

In Figure 3, a comparison is shown between the wave -averaged velocity field obtained by the numerical simulation of Test T3C1 carried out by the proposed model, and the experimental measurements. It can be noted that in the simulated velocity field two eddies are present, close to the T-head groin. It is possible to notice that the wave-averaged velocity field obtained by numerical simulation is in good agreement with respect to the experimental measurements.

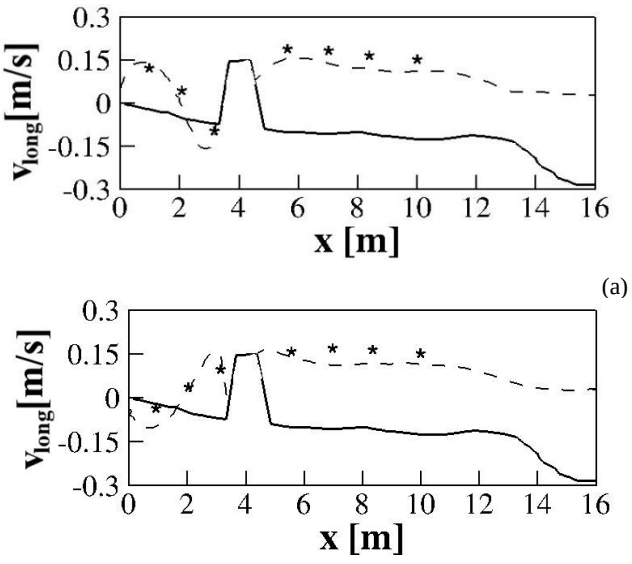

Figure 4 Comparison of calculated (dashed line) and measured (asterisks) longshore currents for Test T3C1 (beach profile in solid line).

Figure 4 shows the comparison between the longshore current (at the two sections shown in Figure 1) obtained by the numerical model proposed in this paper and the experimental measurements by Gravens and Wang [17]. From Figure 4, it can be noted that the numerical results are in good agreement with respect to the experimental measurements.

Figure 5 shows the comparison between the cross-shore current (at the two sections shown in Figure 1) obtained by the numerical model proposed in this paper and the experimental measurements by Gravens and Wang [17]. In these figures, it is possible to notice that the numerical results are in good agreement with respect to the experimental measurements.

In Figure 6, a comparison is shown between the depth contour lines obtained at the end of the numerical simulation of Test T3C1 carried out by the proposed model (black lines), and the corresponding depth contour lines obtained from experimental data by Gravens and Wang [17] (gray lines).

From the comparison between Figures 1 and 6, it can be noted the modification in the bed elevation obtained by the numerical model. From this comparison it is possible to notice a seaward advancement of the shoreline in the lee of the T-head groin and right near the stem: the $0.0 - 0.1m$ depth contour lines advance about 1 m toward the head section. The sediment that is put into suspension in the region upstream of the T-head groin (with respect to longshore current direction) and the sediment coming from the swash zone cause an accretion in the updrift side of the stem: in the lee of the T-head groin, the decay of the current velocity, highlighted by the presence of the above-mentioned first eddy, causes an accumulation of sediment. In the downdrift side of the stem, the rise in the bed elevation is produced by the sediment coming from the swash zone and transported by the second eddy toward the stem.

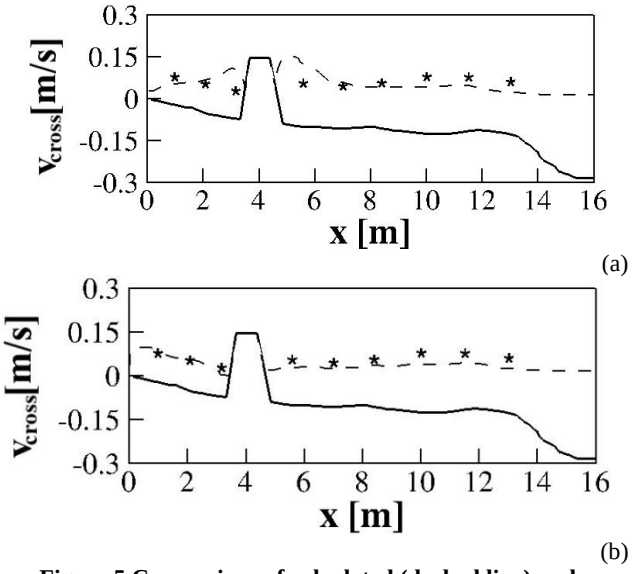

Figure 5 Comparison of calculated (dashed line) and measured (asterisks) cross-shore currents for Test T3Cl (beach profile in solid line).

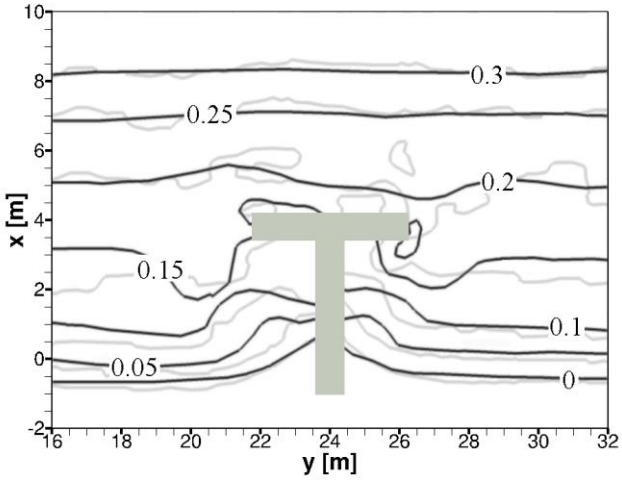

Figure 6 Comparison of calculated (black lines) and measured (grey lines) depth contour lines for Test T3Cl.

From Figure 6, it can be shown the comparison between the measured depth contour lines obtained at the end of the experiment T3C1 and the ones obtained by the proposed numerical model. There is a good agreement between the numerical and experimental results. The presence of the coastal defence structures causes a complex current velocity field, that consistently modifies the local sediment transport. The wave induced longshore current transports the sediment, put into suspension by the breaking waves, up to the region upstream of the T-head groin; in the zone close to the stem of the T-head groin, the current is offshore directed and the sediment are carried towards the lee of the T-head groin, where it settles.

4. CONCLUSION

In this paper, the modifications induced by a T-head groin on the shoreline position and on the bottom, have been simulated by a new numerical model, which is composed by two sub-models: a hydrodynamic model and a morphodynamic model.

From the comparison between the numerical and experimental results it was shown that the proposed numerical models are able to simulate the shoreline and bottom modifications behind a T-head groin.

5. APPENDIX

$$b^l = \vec{g}^{(l)} \cdot \vec{b} \quad ; \quad b_l = \vec{g}_{(l)} \cdot \vec{b} \tag{A1}$$

$$\vec{b} = b^l \vec{g}_{(l)} \; ; \quad \vec{b} = b_l \vec{g}^{(l)} \tag{A2}$$

$$b^l{}_{,m} = \partial\, b^l / \partial\, \xi^m + \Gamma^l_{mk} b^k \tag{A3}$$

$$\Gamma^l_{mk} = \vec{g}^{(l)} \cdot \partial\, \vec{g}_{(k)} / \partial\, \xi^m \tag{A4}$$

$$T^{lm}_{,m} = \frac{1}{\sqrt{g}} \frac{\partial T^{lm} \sqrt{g}}{\partial \xi^m} + T^{nm}\, \Gamma^l_{nm} \tag{A5}$$

6. REFERENCES

[1] Cannata G., Petrelli C., Barsi L., Camilli F. and Gallerano F. 2017. 3D free surface flow simulations based on the integral form of the equations of motion. WSEAS Transactions on Fluid Mechanics. 12, 166–175.

[2] Cannata, G., Gallerano, F., Palleschi, F., Petrelli, C. and Barsi, L. 2019. Three-dimensional numerical simulation of the velocity fields induced by submerged breakwaters. *International Journal of Mechanics*. 13, 2019, 1–14.

[3] Cannata, G., Petrelli, C., Barsi, L. and Gallerano, F. 2019. Numerical integration of the contravariant integral form of the Navier-Stokes equations in time-dependent curvilinear coordinate systems for three-dimensional free surface flows. *Continuum Mechanics and Thermodynamics*, 31, 491-519.

[4] Cannata, G., Barsi, L., Petrelli, C. and Gallerano, F. 2018. Numerical investigation of wave fields and currents in a coastal engineering case study. *WSEAS Transactions on Fluid Mechanics*. 13, 87–94.

[5] Shi, F., Kirby, J.T., Harris, J.C., Geiman, J.D. and Grilli, S.T. 2012. A high-order adaptive time stepping TVD solver for Boussinesq modelling of breaking waves and coastal inundation. *Ocean Modelling*. 43-44, 35-51.

[6] Wei, G., Kirby, J.T., Grilli, S.T. and Subramanya, R. 1995. A fully non-linear Boussinesq model for surface waves. Part 1: Highly nonlinear unsteady waves. *Journal of Fluid Mechanics*. 29, 71-92

[7] Nwogu, O. 1993. Alternative form of Boussinesq equations for nearshore wave propagation. *Journal of Waterway Port, Coastal, and Ocean Engineering*. 119, 618–638.

[8] Chen, Q., Kirby, J.T., Dalrympe, R.A., Shi, F. and Thornton, E.B. 2003. Boussinesq modeling of longshore currents. *Journal of Geophysical Research*. 108, 26-1;26-18.

[9] Chen, Q. 2006. Fully non-linear Boussinesq-type equations for waves and currents over porous beds. *Journal of Engineering Mechanics*. 132(2), 220-230.

[10] Cioffi, F., F. and Gallerano F. 2006. From rooted to floating vegetal species in lagoons as a consequence of the increase of external nutrient load: An analysis by model of the species selection mechanism. *Applied Mathematical Modelling*. 30(1), 10–37.

[11] Drønen, N. and Deigaard, R. 2007. Quasi-three-dimensional modelling of the morphology of longshore bars. *Coastal Engineering*. 54, 197-215.

[12] Kim, N.H. and An, S.H. 2011. Numerical computation of the nearshore current considering wave-current interactions a Gangjeong coastal area Jeju Island, Korea. *Engineering Applications of Computational Fluid Mechanics*. 5, 430-444.

[13] Gallerano, F., Cannata, G. and Lasaponara, F. 2016. A new numerical model for simulations of wave transformation, breaking and long-shore currents in complex coastal regions. *International Journal for Numerical Methods in Fluid*. 80, 571-613.

[14] Gallerano, F., Cannata, G., and Scarpone, S. 2017. Bottom changes in coastal areas with complex shorelines. *Engineering Applications of Computational Fluid Mechanics*. 11(1), 396-416.

[15] Deigaard, R., Fredsøe, J. and Hedegaard, I.B. 1986. Suspendend sediment tin the surf zone. *Journal of Waterway, Port, Coastal, and Ocean Engineering*, 112(1), 115-128.

[16] Rakha, K.A., Deigaard, R. and Brøker, I. 1997. A phase-resolving cross shore sediment transport model for beach profile evolution. *Coastal Engineering*. 31(1-4), 231-261.

[17] Gravens, M.B. and Wang, P. 2007. Data Report: LSTF Experiments — Transport by Waves and Currents & Tombolo Development Behind Headland Structures, Technical Report ERDC/CHLTR-04-9. Coastal and Hydraulics Laboratory. US Army Engineer Research and Development Center Vicksburg MS.